2D X-Ray Radiography of Imploding Capsules at the National Ignition Facility

J. R. Rygg,[1] O. S. Jones,[1] J. E. Field,[1] M. A. Barrios,[1] L. R. Benedetti,[1] G. W. Collins,[1] D. C. Eder,[1] M. J. Edwards,[1] J. L. Kline,[2] J. J. Kroll,[1] O. L. Landen,[1] T. Ma,[1] A. Pak,[1] J. L. Peterson,[1] K. Raman,[1] R. P. J. Town,[1] and D. K. Bradley[1]
[1]*Lawrence Livermore National Laboratory, Livermore, California 94551, USA*
[2]*Los Alamos National Laboratory, Los Alamos, New Mexico 87545, USA*
(Received 25 November 2013; published 12 May 2014)

First measurements of the in-flight shape of imploding inertial confinement fusion (ICF) capsules at the National Ignition Facility (NIF) were obtained by using two-dimensional x-ray radiography. The sequence of area-backlit, time-gated pinhole images is analyzed for implosion velocity, low-mode shape and density asymmetries, and the absolute offset and center-of-mass velocity of the capsule shell. The in-flight shell is often observed to be asymmetric even when the concomitant core self-emission is round. A ~ 15 μm shell asymmetry amplitude of the Y_{40} spherical harmonic mode was observed for standard NIF ICF hohlraums at a shell radius of $\sim$200 μm (capsule at $\sim$5$\times$ radial compression). This asymmetry is mitigated by a $\sim$10% increase in the hohlraum length.

DOI: 10.1103/PhysRevLett.112.195001 PACS numbers: 52.57.Fg, 87.59.B-

In pursuit of inertial confinement fusion (ICF) [1,2] ignition at the National Ignition Facility (NIF) [3], deuterium-tritium (DT) filled spherical capsules are imploded by the x-ray radiation drive produced inside laser-heated cylindrical hohlraums. The capsule shell is rapidly compressed by a radial factor of $\sim$35 to produce a high temperature (>5 keV) central DT hot spot surrounded by cold, dense ($\sim$0.1 keV,$\sim$1 kg/cc) DT fuel. Ignition occurs when energy produced by the hot spot initiates a nuclear burn in the surrounding shell. A high degree of spherical symmetry is required to maximally compress the fuel and heat the hot spot. Any shape distortions as the capsule implodes will diminish the conversion efficiency of the imploding shell kinetic energy; some energy that would convert into thermal energy of the hot spot will instead result in transverse motion of the shell [1,2,4].

The ICF capsule shape is often decomposed into spherical harmonics Y_{lm}, and earlier efforts at the NIF were able to tune out the observed Y_{20} of x-ray self-emission from the core at stagnation (20–35$\times$ compression) [5]. However, the continued presence of residual low-mode ($l \leq 8$) asymmetry in the stagnated shell has been conjectured as a contributor to the degraded fusion yield observed in NIF implosions compared to simulations [6]. In this Letter, we present the first 2D radiography experiments of imploding ignition-scale capsules at peak velocity (3.5–7$\times$ compression) at the NIF and report the measurement and mitigation of a previously undetected low-mode asymmetry in the in-flight capsule shell.

Previous techniques to measure low-mode radiation drive symmetry include early-time drive symmetry using backlit images of thin shells [7–9], shock symmetry using low-density foam balls [10–12], and drive-integrated symmetry using x-ray self-emission of surrogate capsules [13]. More recently on the NIF, related techniques have been used to assess drive symmetry. Radiation symmetry during the first 2–3 ns is measured by imaging the reemission of a bismuth surrogate capsule [14]. Shock symmetry is measured by using a multiaxis laser interferometry technique [15,16]. Time-integrated symmetry is inferred from either the x-ray self-emission [5] or neutron emission [17] from the capsule core at stagnation. Taken together, these techniques provide a partial record of the time-dependent drive symmetry. However, there is a gap in the symmetry diagnosis from the time of the final shock launch to that of stagnation. The technique reported in this Letter provides shape information during this previously undiagnosed epoch of the capsule implosion.

The experimental setup reported herein is an extension of a previously reported technique to measure the time-dependent trajectory of an imploding ICF capsule by using one-dimensional x-ray radiography [18,19]. Our two-dimensional radiography technique also starts with an ignition-scale target modified for backlit imaging (Fig. 1). In this case, the target consists of a cylindrical gold hohlraum with 5.75 mm inner diameter and an inner length between 9.13 and 10.43 mm. A 1.15 mm outer radius, 0.21 mm thick plastic spherical shell is held at the center of the hohlraum by two thin ($\sim$45 nm) plastic membranes. The capsule shell is filled with 6.7 mg/cm^3 of 30 at.% D_2 and 70 at.% ^{3}He gas when cooled to 24 K [20]. The hohlraum is driven with a 1.3 MJ, 21 ns long, four-shock ignition pulse (Fig. 1).

Eight of NIF's 192 beams are redirected from the hohlraum to a germanium foil 12 mm from the capsule center in the equatorial plane. The backlighter (BL) material is chosen so its x-ray emission will have $\sim$1 optical depth through the in-flight capsule shell. To partially compensate for the eight missing BL beams, power is increased by an average of 12.5% on 64 nearby beams. The pulse shape of the BL beams is tuned for best 10.25 keV Ge He-α

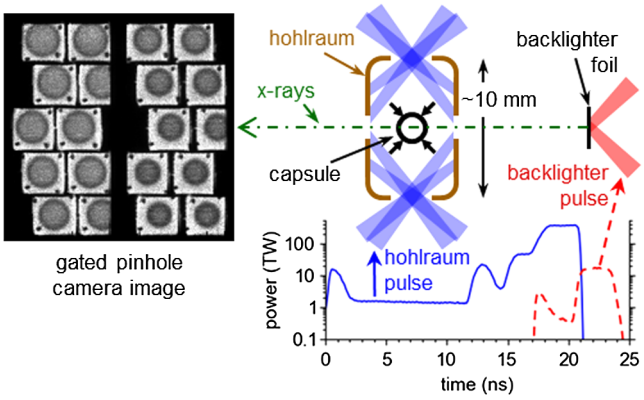

FIG. 1 (color online). A cylindrical hohlraum converts 1.3 MJ of laser energy into a ~ 300 eV radiation drive, imploding the spherical capsule. A backlighter foil is illuminated as the capsule implodes, generating backlit images of the in-flight capsule on a time-gated pinhole camera.

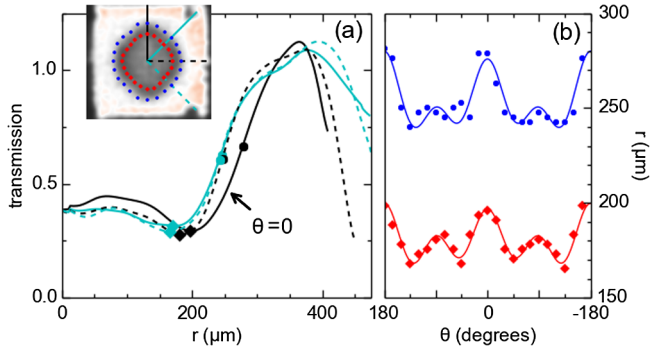

FIG. 2 (color online). (a) Radial lineouts of frame (inset) sectors are analyzed for radii corresponding to the limb minimum (diamonds) and max slope (circles). (b) Limb minimum and maximum slope contours are each fit with a Legendre polynomial series to characterize the low-mode shape of the in-flight capsule shell.

conversion efficiency, as discussed in Refs. [21,22]. The BL's 52 kJ laser energy is converted with about 1% efficiency into the Ge He-α line, creating an x-ray emission area approximately 1 mm in diameter and 2 ns in duration.

To provide a line of sight from the BL foil through the capsule to the detector, two 0.9×0.83 mm viewing holes are cut out of opposite sides of the hohlraum wall. Two 0.8 mm square high-density carbon (HDC) windows are inserted into the cutouts to prevent premature closure of the viewing holes [23]. Low-transmission fiducial dots, ~0.1 mm in diameter, are placed in the corners of the windows to relate the absolute position of the imploding capsule to its initial position.

Area-backlit images of the imploding capsule (Fig. 1) are created by pinhole projection onto a gated x-ray detector [24] at 8× magnification. The detector has two microchannel plate (MCP) striplines with a temporal integration time of ~90 ps. The MCP strips and BL pulse are timed to coincide with capsule radii between 300 and 150 μm. Discrete image frames are generated through an array of 20 μm diameter pinholes. The pinhole diameter limits the system resolution to 23 μm in the capsule plane. Often visible is a pair of horizontal bands at approximately half the capsule radius; these are seeded by the plastic membranes that initially hold the capsule at the center of the hohlraum [25].

Data images consist of multiple time-gated image frames generated by these individual pinholes. The image frame intensities are converted to capsule transmission by using pinhole tomography. The tomographic method takes advantage of the slight parallax difference between the backlighter and capsule object planes for each pinhole in the pinhole array to distinguish features originating in the respective planes.

The shape of imploding ICF capsules is often decomposed into spherical harmonics Y_{lm}, the azimuthally symmetric of which (Y_{l0}) are represented by Legendre polynomials P_l. To evaluate the shape of the in-flight shell, each frame is divided into angular sectors, and the radial lineout for each sector is analyzed for the limb minimum and maximum slope radii [Fig. 2(a)]. These radii correspond approximately to the inner and outer boundaries of the shell, respectively. The contours constructed from these radii are each fit with a Legendre polynomial series [Fig. 2(b)] [26]:

$$r(\theta) = \sum_l A_l P_l(\cos\theta).$$

The fit averages over any left-right asymmetry, which is typically smaller than the fit uncertainty. Odd modes are expected to be small due to the up-down symmetry of the hohlraum drive, and even mode amplitudes are expected to diminish with higher mode number due to increasingly effective smoothing from the radiation drive [1]. The imaging system resolution limits the mode sensitivity to $l \leq 10$.

Evolution of the low-mode capsule shape as it implodes, including the dA_0/dt "implosion velocity," is obtained by sequential analysis of the image frames. Areal density can be inferred from the capsule transmission with a suitable assumption of the shell opacity [18,19], giving a typical areal density of ~0.1 g/cm^2 at the time of the radiograph. Detailed results of the areal density symmetry analysis for the 2D radiographs will be reported elsewhere.

Additionally, the spatially and temporally resolved radiograph is used to measure a capsule center-of-mass (c.m.) velocity, which could be imparted by unintentional large asymmetries in the radiation flux. The absolute position and c.m. velocity of the capsule are measured in reference to the fiducial dots placed on the HDC windows [27]. Comparison of the absolute position of the capsule over the ~0.4 ns frame sequence allows us to constrain the c.m.

velocity of the capsule to ~10 km/s. Typically, the c.m. of the imploding capsule is within 15 μm of the initial capsule center (P_1 is the vertical component of this offset) and is moving with a speed less than 20 km/s within the plane transverse to the line of sight. The associated c.m. kinetic energy represents less than 1% of the kinetic energy of the ~285 km/s imploding shell.

As a first demonstration of this NIF 2D radiography platform, a campaign was undertaken which confirmed the conjectured presence of an in-flight P_4 distortion of the shell [6]. In this conjectured scenario, the observed hot-spot self-emission symmetry could still appear round due to a mixture of various low-mode components in the shell. Previous experiments had tuned out low-mode shape perturbations based on the hot-spot self-emission measurements and selected a hohlraum length of 9.43 mm to produce optimal control of P_2 asymmetry for a hohlraum inner diameter of 5.75 mm [15]. However, the symmetry of the assembled cold fuel could not be conclusively demonstrated without a direct measurement of the shell; this 2D radiography platform was used to make such a measurement at the NIF.

To evaluate the shell symmetry, a sequence of otherwise-identical shots was performed in which the hohlraum length varied from 9.13 to 10.43 mm. The outer cone beams were kept at the same position with respect to the laser entrance holes (LEHs) by repointing them by half the difference in hohlraum length. The 64 inner cone beams kept the same pointing near the hohlraum midplane, independent of hohlraum length. The shell implosion velocity is the same for all experiments in this campaign at 285 $\pm$ 12 km/s and is constant for the ~0.4 ns duration of the radiographic window. In addition to the in-flight 2D radiography measurement, time-integrated self-emission [28] images were measured concomitantly from the same line of sight.

As seen in Fig. 3, the shape of the in-flight capsule shell often differs dramatically from the shape of the x-ray emission from the stagnated core. In particular, the short (9.13 mm) hohlraum experiment results in an imploding shell that primarily exhibits a positive P_4 [Figs. 3(a) and 3(c)], whereas the resultant self-emission is dominated by a negative P_2 [Fig. 3(e)]. This result suggests that contours of the self-emission are not reflective of the shape of the stagnated ablator shell.

For the experiments in this study, odd modes ($l > 1$) are always consistent with zero (± 2 μm), and higher even modes ($l > 4$) are generally small (<3 μm amplitude), except in cases where both A_2 and A_4 are >10 μm, for which even-mode mixing generates ~5 μm of A_6 and A_8. As previously reported for self-emission measurements [5], P_2 can be independently controlled through the cross-beam energy transfer (CBET) mechanism. The amount of energy transferred between inner and outer laser beams by a plasma wave self-generated where the beams cross near the LEHs [30] depends in part on the difference in their laser wavelength $\Delta\lambda$. For the in-flight shell, a reduction of the measured A_2 from 25 to 1 μm was observed with an adjustment of 0.21 nm in $\Delta\lambda$.

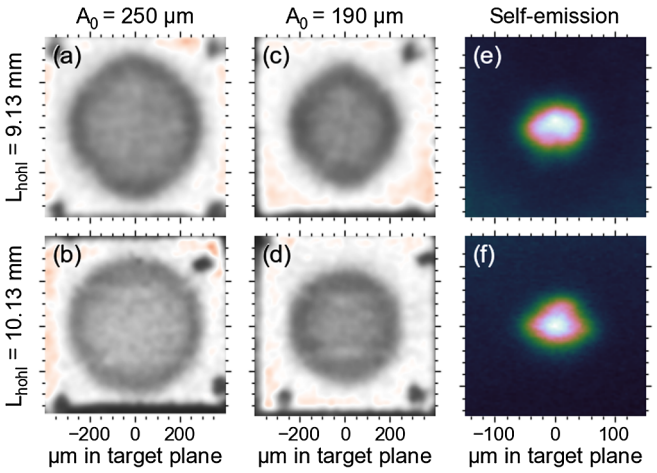

FIG. 3 (color online). (a)–(d) Radiographs of the capsule in flight at $A_{0,\mathrm{limbmin}} = 250$ and 190 μm (0.72 and 0.51 ns before stagnation, respectively). A ~ 17 μm A_4 component is reduced below 5 μm with the ~10% longer hohlraum. (e),(f) Concomitant time-integrated self-emission images often exhibit a different low-mode shape than the in-flight shell radiographs. Note the change in spatial scale for (e),(f).

Figure 4(a) shows the radial evolution of the A_4 fit parameter to the limb-minimum contour as the capsule implodes. The ~6 μm increase in A_4 as the capsule implodes over the ~0.4 ns time window of the measurement indicates a P_4 swing rate of ~15 μm/ns. This observed P_4 swing rate is not strongly correlated with hohlraum length.

Shown in Fig. 4(b) is the dependence of A_4 on hohlraum length. A shell A_4 of 13 μm is observed for the 9.43 mm length hohlraum experiment when the capsule radius is at

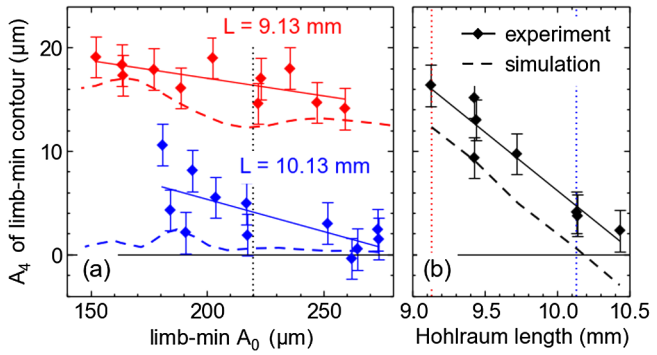

FIG. 4 (color online). (a) Evolution of the capsule shape as it implodes over ~0.4 ns for two different hohlraum lengths L. (b) In-flight capsule A_4 at $A_0 = 220$ μm is reduced to within 5 μm of "round" for L approximately 1 mm longer than the previous standard. Solid lines are linear fits to the data. Hydrodynamic simulations (dashed lines) get the correct scaling of A_4 with L, but with an offset in the absolute A_4 amplitude.

220 μm (~0.6 ns before shell stagnation). The residual P_4 asymmetry is mitigated by an ~1 mm increase in hohlraum length.

The scaling of the in-flight P_4 with hohlraum length can be understood qualitatively by using a simplified spherical model of the hohlraum [1]. In this model, the P_4 component of the radiation flux seen by the capsule is a balance of contributions from the laser-heated emission rings and the reradiation from the hohlraum wall. As the hohlraum is lengthened and the outer rings move outwards, the outer rings increase the P_4 contribution to the capsule radiation flux. The in-flight shape responds to low-mode flux asymmetries with opposite sign, as the higher flux regions are driven to smaller radius, reducing in-flight P_4. However, this time-independent model cannot explain the observed P_4 swing.

To better understand the cause of the P_4 swing as well as the observed change due to hohlraum length, simulations were done by using the radiation hydrodynamics code HYDRA [29]. The hohlraum and capsule are calculated together in a self-consistent calculation, where the laser refraction, absorption, and subsequent conversion to x rays near the gold hohlraum wall are calculated directly, and those x rays then are transported to the capsule ablation surface and drive the capsule inwards. CBET is modeled in a separate calculation [30] using plasma parameters extracted from the initial HYDRA simulation. A second HYDRA calculation is then done with the input laser power adjusted by the measured laser backscatter and calculated CBET and further modified in order to match shock timing, trajectory, and neutron bang time data from other experiments [31].

These axisymmetric HYDRA simulations reproduce the observed scaling of the in-flight capsule P_4 with hohlraum length but have an offset as to the absolute magnitude [Fig. 4(b)] [23]. Simulations anticipate that the P_4 time-dependent swing is reduced for longer hohlraums, in contrast to the measurements which demonstrate no such reduction.

The underlying cause of the difference between the in-flight and self-emission shape is an area of active investigation. The HYDRA model of the implosion, which is designed to match the observed symmetry up through the in-flight shape measurement, can provide insight into the evolution of the shell and hot spot at stagnation. Figures 5(a) and 5(b) show simulated transmission images for the 9.13 and 10.13 mm hohlraums, respectively, that agree with the measured radiographs in Fig. 3. The shell density and temperature at the time of shell stagnation is shown in Figs. 5(c) and 5(d). These simulations indicate that there should be significant mass accumulation near the poles and that this flow causes the core self-emission P_2 shape to diverge markedly from the in-flight shape, especially for the 10.13 mm hohlraum.

Note that these simulations do not include the effect of the capsule membrane, which is observed to seed horizontal

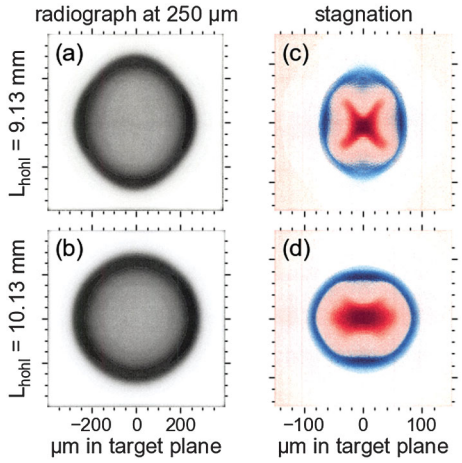

FIG. 5 (color). Postshot hydrodynamic simulations of experiments shown in Fig. 4. (a),(b) The 10.25 keV x-ray transmission of the in-flight capsule at 250 μm shell radius. (c),(d) Density (blue) and temperature (red) cross section of the stagnated capsule at the time of peak x-ray emission. Self-emission and transmission at stagnation roughly follow the temperature and density contours, respectively. Note the change in spatial scale for (c),(d).

bands in the experimental radiograph [25]. We conjecture that the band seeded by the membrane is further amplified at stagnation, causing the core temperature to quench in regions ~45° from the poles, with a corresponding effect on the self-emission shape.

In summary, a new experimental platform was developed at the NIF for 2D radiography of imploding capsules in flight. The shape of the hot-spot self-emission was demonstrated to be sometimes misleading as to the symmetry of the surrounding cold shell. The dependence of the in-flight shape on hohlraum length was measured, and the optimum length to minimize spherical harmonic Y_{40} was determined to be ~10% longer than the previous standard, chosen based on self-emission shape measurements. Residual temporal swings in the low modes remain. Results from this platform are being used in an ongoing manner to improve several models used in ICF simulation and design codes and to determine the implosion velocity, c.m. velocity, areal density, and low-mode shape of the imploding capsule shell for new ICF configurations at the NIF.

The authors thank the engineering, target fabrication, and operations teams at the National Ignition Facility who made these experiments possible. This work was performed under the auspices of the U.S. Department of Energy by Lawrence Livermore National Laboratory under Contract No. DE-AC52-07NA27344.

[1] J. Lindl, Phys. Plasmas **2**, 3933 (1995); **11**, 339 (2004).
[2] S. Atzeni and J. Meyer-ter-Vehn, *The Physics of Inertial Fusion* (Oxford University, New York, 2007).

[3] G. H. Miller, E. I. Moses, and C. R. Wuest, Nucl. Fusion **44**, S228 (2004).
[4] A. L. Kritcher *et al.*, Phys. Plasmas **21**, 042708 (2014).
[5] S. H. Glenzer *et al.*, Science **327**, 1228 (2010).
[6] R. H. H. Scott *et al.*, Phys. Rev. Lett. **110**, 075001 (2013).
[7] D. H. Kalantar, S. W. Haan, B. A. Hammel, C. J. Keane, O. L. Landen, and D. H. Munro, Rev. Sci. Instrum. **68**, 814 (1997).
[8] S Pollaine, D. K. Bradley, O. L. Landen, R. J. Wallace, O. S. Jones, P. A. Amendt, L. J. Suter, and R. E. Turner, Phys. Plasmas **8**, 2357 (2001).
[9] R. Kirkwood *et al.*, Phys. Plasmas **16**, 012702 (2009).
[10] P. A. Amendt, S.G. Glendinning, B.A. Hammel, O. Landen, and L.J. Suter, Phys. Rev. Lett. **77**, 3815 (1996).
[11] S. G. Glendinning *et al.*, Rev. Sci. Instrum. **70**, 536 (1999).
[12] R. E. Turner, P. A. Amendt, O. L. Landen, L. J. Suter, R. J. Wallace, and B. A. Hammel, Phys. Plasmas **10**, 2429 (2003)
[13] P. Amendt, T. J. Murphy, and S. P. Hatchett, Phys. Plasmas **3**, 4166 (1996).
[14] E. L. Dewald *et al.*, Phys. Rev. Lett. **111**, 235001 (2013).
[15] D. A. Callahan *et al.*, Phys. Plasmas **19**, 056305 (2012).
[16] J. D. Moody *et al.* (to be published).
[17] G. P. Grim *et al.*, Phys. Plasmas **20**, 056320 (2013).
[18] D. G. Hicks, B. K. Spears, D. G. Braun, R. E. Olson, C. M. Sorce, P. M. Celliers, G. W. Collins, and O. L. Landen, Phys. Plasmas **17**, 102703 (2010).
[19] D. G. Hicks *et al.*, Phys. Plasmas **19**, 122702 (2012).
[20] These D^3He-filled symcap capsules are designed to have the same rocket behavior as the cryogenic DT ignition capsules (yet be more practical to field) by replacing the DT ice layer by an equal mass of plastic. Both the simple rocket model and hydrodynamic simulations show that symcaps have the same in-flight response to the radiation drive. The fusion yield in these symcaps is insensitive to the symmetry changes made here. The shape is expected to affect the yield performance of layered capsules that sit near the "ignition cliff".
[21] D. Babonneau *et al.*, Phys. Plasmas **15**, 092702 (2008).
[22] M. A. Barrios, K. B. Fournier, S. P. Regan, O. Landen, M. May, Y. P. Opachich, K. Widmann, D. K. Bradley, and G. W. Collins, High Energy Density Phys. **9**, 626 (2013).
[23] The viewing holes introduce an azimuthal asymmetry compared to the windowless case. However, this "M_2" asymmetry is aligned along the radiographic lineofsight and 3D calculations with and without the windows show the difference in the observable polar asymmetries isless than the experimental uncertainty.
[24] J. A. Oertel *et al.*, Rev. Sci. Instrum. **77**, 10E308 (2006).
[25] The membrane was conclusively identified as the origin of these bands by two independent sets of experiments, to be published elsewhere. In most cases, this feature has only a small effect on the inferred in-flight shape.
[26] The Legendre-mode shape breakdown is insensitive to the application of the tomographic step.
[27] Only the components of position and velocity transverse to the line of sight are directly observed.
[28] T. Ma *et al.*, Rev. Sci. Instrum. **83**, 10E115 (2012).
[29] M. M. Marinak, G. D. Kerbel, N. A. Gentile, O. Jones, D. Munro, S. Pollaine, T. R. Dittrich, and S. W. Haan, Phys. Plasmas **8**, 2275 (2001).
[30] P. Michel *et al.*, Phys. Plasmas **17**, 056305 (2010).
[31] O. S. Jones *et al.*, Phys. Plasmas **19**, 056315 (2012).